The Effect of Tree Shade and Snowpack Cover on Pavement Surface Temperature

A Thesis

SUBMITTED TO THE FACULTY OF THE

UNIVERSITY OF MINNESOTA

BY

Nahum Denisovich Yelizarov

IN PARTIAL FULFILLMENT OF THE REQUIREMENTS FOR

THE DEGREE OF MASTER OF SCIENCE

Advisor: Dr. Mihai Marasteanu

June 2023

ACKNOWLEDGEMENTS

I would firstly like to express my deepest appreciation to my advisor, Dr. Mihai Marasteanu, for his continuous and generous support, encouragement, and assistance throughout my undergraduate and graduate careers at the University of Minnesota. I am also extremely grateful to the other committee members, Dr. Xue Feng and Dr. Yingling Fan, for their time and their contributions to this thesis and the defense process. Additionally, this endeavor would not have been possible without the generous financial support from the MSES/MAPA Fellowship.

I also need to give special thanks to all the individuals who gave me their time and provided me with advice and expertise. Thanks go to:

- Dr. Vaughan Voller for his help with the modeling aspects of this thesis.
- Mugurel Turos for his support throughout my academic endeavors and his numerous suggestions in my research.
- Dr. Eyoab Zageye and Thomas Calhoon for their efforts in data collection and analysis.

I would also like to thank my friends and family for their love, support, and patience during my time as a graduate student and for always being there for me when I need it.

ABSTRACT

The effects of tree shade on the surface and internal temperature of pavement structures can be significant throughout the year. While much work has been done in researching the influence of tree cover on localized urban heating during hot summer months, less effort has been put towards the research of the effects of tree shade on pavement heat transfer during cold weather. A recent road project in Minnesota has resulted in increased interest in the balance of sun exposure and minimum pavement surface temperatures for winter road maintenance. This thesis provides an extensive literature review on tree cover and methods of calculating shade, winter maintenance practices, principles of heat transfer for snowpack systems, and the urban heat island effect. Then, a 1D heat transfer model, combining snowpack systems and pavement structures, is developed and presented, and a sensitivity analysis is performed on several model parameters. Finally, recommendations are made for future work, including field measurements at the project site, and implementation of the model for consideration in selective tree removal.

TABLE OF CONTENTS

LIST OF TABLES

LIST OF FIGURES

CHAPTER 1: BACKGROUND

Pavement surface and internal temperature are important factors which affect the near-surface air temperature. Pavement temperature plays an important role in pavement design, mitigation of the urban heat island (UHI) effect, and winter maintenance. Pavement structures absorb and store a large amount of heat during the day and release it during the evening and night. This diurnal cycle causes increases in temperature of the near-surface air and increases the sensible heat flux **[1]**. During winter in northern climates, higher surface temperature is beneficial in keeping roads clear of snow and ice for users. During summer, higher surface temperatures can increase air temperatures in urban environments and contribute to the negative effects of the urban heat island effect. Tree shade affects the surface temperature through both direct shading and redirection of the energy budget to evapotranspiration. Therefore, it is important to understand the climatic variables and thermal properties of pavements that affect the heat transfer process in pavement structures and explore the effect tree shade can have on the heat transfer process for pavement structures throughout the year.

While the effects of pavements and tree cover related to the heat island effect have received considerable attention, research on the effect of tree shade on pavement temperatures during cold winter months has been less studied. Minnesota Department of Transportation (MnDOT) District 4 engineers are interested in understanding the balance of optimal sun exposure and selective tree cutting as part of a new road project. This project involves full depth reclamation and resurfacing of a 21-mile road segment on Trunk Highway 34, from Becker County Road 29 to just west of Osage, in the summer of 2023. As part of this project, clear zone tree removal was performed in March 2023 on both sides of the road. Selective logging is also planned in the fall and winter of 2024-2025 to reduce the shading on the highway that causes cold spots during wintertime. Understanding the effects of tree shading on pavements is necessary to help ensure only the necessary removal of trees to improve road safety of users.

Objectives and Research Approach

To better understand the effects of tree shade on pavement surface temperature, a literature review covering the influence of tree cover on sun exposure and methods to calculate that influence, road winter maintenance practices and snowpack heat transfer, and the urban heat island effect is conducted. A 1D numerical heat transfer model that includes snow melting processes is developed by combining existing snowmelt and pavement models and including a tree shade factor for incoming energy fluxes. The model is tested using historic weather conditions and compared to thermocouple data. Additional data collection efforts on sunlight exposure and pavement temperature are also explored and discussed. Recommendations for the future efforts for the project are included at the end of this thesis.

CHAPTER 2: LITERATURE REVIEW

2.1 Tree Cover

The effect of trees on the surface temperature is a complex process involving interception of precipitation, direct shading of the ground surface, and evapotranspiration. These effects are heavily dependent on the types of trees and the seasonality. For urban areas, tree canopy size, density, leaf area index (LAI), and stress tolerance are all important factors for the cooling effectiveness of evapotranspiration **[2]**. The effect of trees on air and surface temperature is dependent on tree species. Urban tree species with higher LAI, sapwood area, and sap-flux density have higher transpiration and more cooling through direct shading **[3]**. A model developed by Napoli (2016) **[4]** following work by Liu and Jordan (1960) **[5]** separates incoming solar radiation into diffused and direct radiation as a function of a "clearness index". This model calculated canopy transmittance as a function of LAI and vegetation dependent attenuation coefficient. The seasonal cycle of deciduous trees directly affects all the processes mentioned above. The amount of solar radiation blocked by a canopy at full leaf condition has been found to be around two times higher than that during wintertime conditions **[6]**.

The degree of solar attenuation due to shading has been explored by Yates and McKennan (1989) where light attenuation percentage for different trees during winter and summer were compared and various methods of measurement were discussed. Methods included measuring solar radiation directly using a pyranometer or light meter and measuring crown density using canopy photograph analysis using dot matrix or video-scanning. Attenuation percentage is heavily dependent on the method used which results in a lot of wide discrepancies in the results in literature. Yates and McKennan focused on using a dot matrix to measure crown density as this method is a very simple method for estimation of tree to sky, especially during wintertime when diffuse radiation through the canopy is low **[7]**. The results of the dot matrix gave very close estimates of crown transmittance to those measured directly by a luminance meter. The regular dot matrix procedure of rating winter crown density was first developed by Wagar and Heisler (1986) **[8]**. This method is very easy to use and can be directly applied to a specific site.

Numerical simulation has also been used to calculate solar transmittance of trees. A study done by Kumakura et al. (2013) modeled five deciduous tree species using computer aided design and calculated surface temperature near the trees to compare the solar shading effects in both summer and winter. Direct solar radiation and sky solar (reflected) radiation transmittance was calculated and integrated at an incident angle of tree crown from 0 to 90 degrees. During wintertime, direct solar radiation transmittance was between 40-80% and sky solar radiation transmittance was between 30-45%. Direct solar radiation for a tree species varied with the incident angle **[9]**.

A study done by Gardner and Sydnor (1984) used pyranometers to measure direct and diffuse solar radiation transmitted through five species of trees at Ohio State University. The average percentage of shade was measured in summer and winter months. Between December and March, the mean shade varied from 10-40%. The variability was between the different species of trees and was related to canopy density and shape of the crown **[10]**.

Heisler (1986) also looked at how four species of deciduous trees in Pennsylvania reduced the solar irradiance on buildings. The tree dimensions and crown densities were measured and pyranometers were used to measure radiation reduction. Measurements for percentage reduction were done for unshaded and shaded points on the wall in both winter and summer months. For shaded regions, the percent reduction in wintertime was found to be between 20-45% and relationships were empirically determined for irradiance reduction as a function of the fraction of diffuse radiation for both in-leaf and leafless conditions **[11]**.

Bueno-Bartholomei and Labaki (2003) used solarimeters to calculate incident solar radiation attenuation beneath tree crowns and in open areas. Attenuation was calculated as a fraction of areas giving total incident energy in sunlight minus areas of total incident energy in shade over the areas in sunlight. The results were also normalized for ambient temperature for the study days. The tree species analyzed are common to Brazil. Measurements were made during wintertime for two of the species in the study, with the variation in attenuation results directly attributed to specific characteristics of the tree species **[12]**.

A study by Konarska et al. (2014) specifically focused on the reduction of solar radiation during wintertime in the leafless condition. The study measured the transmissivity of solar radiation

using pyranometers for four deciduous tree species and a coniferous tree species common to Northern Europe. Total and direct solar radiation was calculated at a reference point and below the trees and the transmittance ratio was determined. Results for in-leaf and leafless conditions were compared. The results were correlated with the sky view factors determined from fish-eye photographs taken of the tree canopies. Empirical relationships were made between the sky view factors and the transmissivity for the tree species. The study found that for the leafless condition, transmissivity of solar radiation was highly variable with time of day **[13]**.

McPherson et al. (2018) calculated the percentage of sky covered by the tree crown, or shade factors, for 149 tree species common to 17 U.S. cities. Shade factors can be used for modeling effects of solar radiation attenuation, precipitation interception, and air pollutant intake. The shade factors were determined using photographs of the tree crowns and comparing the pixels representing foliage and branches to total area of the crown silhouette. They developed nonlinear relationships to calculate shade factors as a function of diameter at breast height and tree age, and climate effects **[14]**.

It is also important to understand the contribution of cooling due to evapotranspiration compared to cooling due to shading. The relative amount of cooling by each mechanism is found to be scale dependent. At the small scale of a single canopy, evapotranspiration was found to have a lower effect on reducing air temperature within and below the canopy than above the canopy (about 10% of total cooling) **[15]**, however this is not necessarily a universal phenomenon. At the scale of an urban green area like an avenue or a green square, the cooling effect was found to be 80% due to tree shading rather than evapotranspiration **[16]**. At large spatial scales, evapotranspiration accounts for about half of the solar energy absorbed by land surfaces **[17]**. Based on the reviewed literature, for selective cutting of trees to reduce shade, the change in the cooling due to evapotranspiration is not expected to be significant.

2.2 Winter Maintenance

During cold weather events, ice and snow can accumulate on the pavement surface. This can cause slippery and dangerous conditions for users. Removing this accumulation is the most important action for road winter management. The most common method for deicing road

surfaces is by salting **[18]**. Sodium chloride (NaCl) and other chloride deicing chemicals act as freeze-point depressants to melt ice at a lower temperature. An investigation of the thermodynamics of ice melting with the use of deicers has been explored experimentally and is able to be predicted reasonably well **[19]**. Sodium chloride has a high ice melting efficiency at -3^{o}C which decreases as the surface temperature lowers. It is ineffective at melting ice below -15^{o}C **[20]**.

The amount of deicing chemicals needed to melt ice on roads increases as pavement surface temperature decreases. The Minnesota Snow and Ice Control handbook lists the number of pounds of ice melted per pound of salt, decreasing from 46.3 pounds of ice at 30^{o}F to 6.3 pounds of ice at 15^{o}F. At temperature below 15^{o}F, dry salt is found to be ineffective **[21]**. Excess use of chloride deicers has many significant negative impacts to the infrastructure and the environment. Deicers cause degradation and loss of durability of concrete pavements and corrosion of bridges, highway maintenance equipment, and vehicles **[22], [23]**. Environmental impacts include increased accumulation of chloride and increased salinity in runoff water, density stratification and reduced oxygen in aquatic systems, high concentration of chloride salts in soil, and reduction of plant growth and increased erosion **[24]**.

Optimizing the amount and efficiency of deicing chemicals helps in reducing both negative impacts of these chemicals and the costs associated with winter maintenance. Slope data and snowmelt rates can be used to optimize deicer distribution to target areas that are most vulnerable based on amount of incident solar radiation and available weather data **[25]**. Incoming solar radiation can be estimated using meteorological models, such as the one described by Nuijten (2016) in the prediction of airport runway temperature. This model considers insulation by the atmosphere and cloud cover **[26]**.

Numerical models which use weather data to predict pavement temperatures such as the one-dimensional model described by Shao and Lister (1996) **[27]** can be useful in optimizing winter maintenance by providing short-term forecasting. These models can be validated and calibrated with existing pavement temperature sensors. A comprehensive review of existing models for pavement temperature prediction is described Chen et al. (2019) **[28]**.

Pavement surface temperature variations between sun-exposed and shaded sites are of considerable magnitude and should be considered; shading is especially important for cold clear weather with light wind, as found by Bogren et al. (2000) **[29]**. Typical ways to find the sky view factors is using photographs made by a 360^{o} camera with a fish-eye lens, Google Street View, and digital elevation and surface models **[30]**. A study done in Finland included a sky view factor and local horizon angles in an existing road weather model to include the effects of shading by buildings and trees. This study used road weather stations to calculate the factors and angles, however, the vague locations of the road weather stations made the calculations inaccurate because the sky view factor and local horizon angle were found to be very dependent on the exact location **[31]**.

2.3 Snowmelt Heat Transfer

The heat transfer process of snowpacks is a complicated dynamic process which significantly varies with the age of the snow and climatic conditions. Snow is a granular porous material, which can be a two-phase or three-phase system, depending on its temperature. Below the melting point of ice, the pore spaces in the snowpack contain air, however, when the temperature is above the melting point, part of the snow melts and the pores can contain liquid water. The energy balance of a snowpack consists of the net flux of energy from the atmosphere and ground equal to the melt energy flux plus change in internal energy. When the net input of energy is negative, this is the accumulation period when the snowpack forms. Once the net input energy becomes positive, the snowpack enters the melt period, divided into the warming phase, ripening phase, and output phase. This progression isn't necessarily uniform; during periods of time when temperature is above 0 degrees Celsius, melting at the snowpack surface can occur. This water can percolate back into the snowpack and refreeze **[32]**.

There are many temperature models for snow cover that exist. A one-dimensional model developed by Jordan **[33]** is a comprehensive energy balance model for low level flow which models the seasonal snow cover beginning with ground freezing during fall up to the freeze-thaw cycles occurring in spring. A snow accumulation and ablation model called SNOW-17 **[34]** is a simplified one-dimensional point source model which uses air temperature and precipitation as

the only climatic variables for the energy exchange at the snow-air surface. Both values can be readily available from public weather data.

A simplification can be made when considering the properties of snow for the energy transfer. Surface condition categories can be used to attribute emissivity coefficients and albedo values to hoarfrost, dry and wet pavements, dry and wet snow, slush, and ice, as described by Nuijten (2016) **[26]**. Mass balance of water, snow, and ice must be performed to calculate the energy fluxes due to phase changes of water, surface runoff, evaporation, and snow removal associated with winter maintenance.

2.4 Urban Heat Island Effect

Urban development leads to an increase in near-surface temperatures. The change of pre-existing natural environment to urban infrastructure results in local hotspots, as evident in Phoenix, Arizona **[35]**. Mesoscale remote sensing and microscale thermography show that pavements significantly contribute to the increased surface temperatures. These tools can be used to study the variability in heating effects related to material type and spatial patterns **[36]**. Pavements have a lower albedo and higher heat storage capacity than native vegetation, and lead to local atmospheric heating processes **[1]**. These heating processes, known as the urban heat island (UHI) effects, have many potential negative impacts. These impacts include increase in energy use, impaired water and air quality, compromised human health and comfort, and deterioration of pavements **[3]**.

There are different strategies for UHI mitigation. Tree canopy cover can affect the radiation heat flux that occurs at the pavement surface. Vegetation uses solar radiation and converts the energy to latent energy associated with evapotranspiration. Urban trees can be used to reduce the UHI effect caused by pavements in cities. By blocking the shortwave radiation, the pavement temperature can get significantly reduced **[4]**. This reduction in surface temperature can also lead to improvement of performance. Higher pavement condition has been statistically correlated to more tree shading, resulting in reduced pavement distress like fatigue cracking, rutting, and shoving **[37]**.

A systematic review to evaluate different urban tree species' characteristics was performed by Rahman et al. (2020) **[38]** to suggest the relative strength of cooling benefits caused by various variables. This study looked at a subset of studies of single or small clusters of trees in different climates and under different growth conditions. The study found that the benefits of shading were most reliant on the climate of the site and the type of surface below the trees. General planting guidelines were provided which emphasized higher canopy density, particularly at the lower crown, and mixing tree species for layering canopies, and using species with dark green leaves and higher sap wood area will provide better cooling of surfaces.

Other methods for reducing the UHI effect include modifying pavement material thermal properties, enhancing directional thermal conductivity, and utilizing reflective surfaces. Increasing albedo of paving surfaces by using reflective materials, increasing pavement permeability, increasing thermal storage capacity by using materials with high thermal capacitance have all been used to effectively decrease the release of heat at the near surface **[39]-[45]**.

CHAPTER 3: DISCUSSION OF MNROAD AND ROAD DOCTOR DATA

3.1 MnROAD Data

Operated by the Minnesota Department of Transportation, MnROAD is a test track facility located near Albertville, Minnesota. The facility works in conjunction with the Office of Materials & Road Research (OMRR). The facility operates in two road segments with over 50 unique test sections. The test sections collect detailed pavement performance data using pavement and environmental sensors. Data collected for the MnROAD projects is stored on the InfoPave database, operated by the Federal Highway Administration **[46]**.

Data collected includes field monitoring of pavement performance in terms of strength, stiffness, distress, noise levels, etc. Materials testing is also done for the tested pavement sections, and the data on aggregates, hot-mix asphalt, and Portland cement concrete is available. Climate data collected at the MnROAD Site Weather Station includes solar radiation, pressure and humidity, precipitation intensity, wind speed and gust, and air temperature. Climate data is collected every quarter-hour. Thermocouples are also installed within each of the test sections, with pavement temperature measurements taken every quarter hour. Traffic data on both high volume and low volume road segments is also recorded.

The extensive amounts of climate and pavement performance data allows for calibration of the model for various pavement structures and weather conditions.

3.2 Road Doctor Data

Operated by the MnDOT Materials & Road Research Lab, the Road Doctor is a vehicle outfitted with an array of sensors and equipment that are used to measure the pavement performance at a specific road site in Minnesota. Equipment includes ground penetrating radar, temperature sensors, roughness and deflection sensors, and others. The portability of the road doctor and the usability of much of the equipment at traffic speeds allows the Road Doctor to be very beneficial to many research applications without the need for traffic control.

The Road Doctor was used to conduct thermal imagery of the pavement surface on Trunk Highway 34 on 10 February 2023. Two runs were performed on the eastbound lane: one at 10:30 AM and one at 2:15 PM, from Becker County Road 29 to County Road 47. Pavement surface temperature is measured in front of the vehicle, with an analysis line selected within the thermal video frame. This setup is shown in Figure 1.

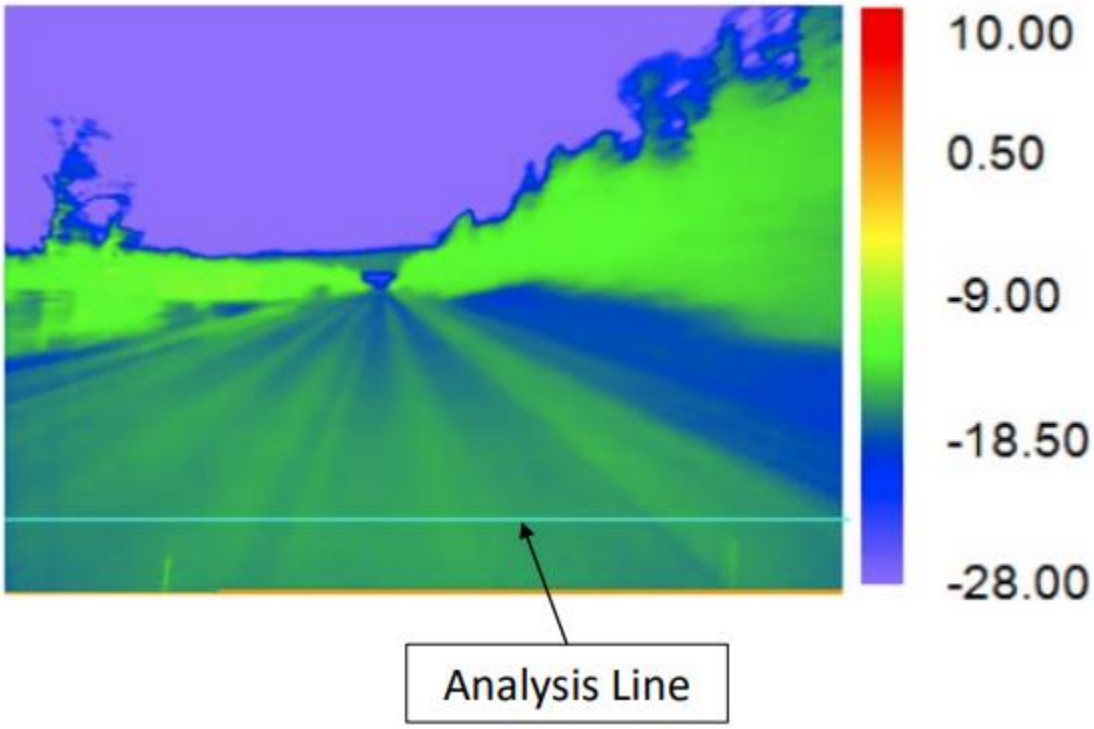

FIGURE 1. THERMAL DATA PROCESSING WITH ANALYSIS LINE.

This line signifies the temperature of a strip of the pavement, several feet in front of the vehicle. As the vehicle travels, this strip moves along the road and the temperature of the entire eastbound lane is collected. The thermal data for the analysis line is exported into an Excel database and can be visualized in a heat map. The resulting heat map shows where there may be hot spots or cold spots within the road segment. The heat map for both runs is shown in Figure 2.

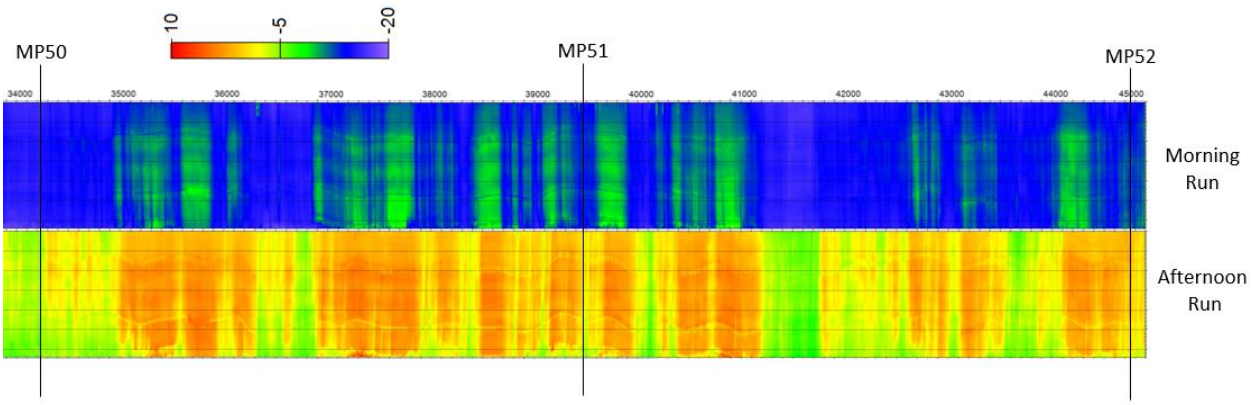

FIGURE 2. EASTBOUND HEAT MAP FOR TH34 BETWEEN MILE POINTS 50 AND 52.

By selecting a point on the analysis line, one can see how the pavement temperature changes at a certain point within the road width throughout the length of the road segment.

By correlating the heat map results with where there is tree shade along the road, it is shown that the thermal data can capture the temperature differential effect of tree shade cover. This is shown in Figure 3.

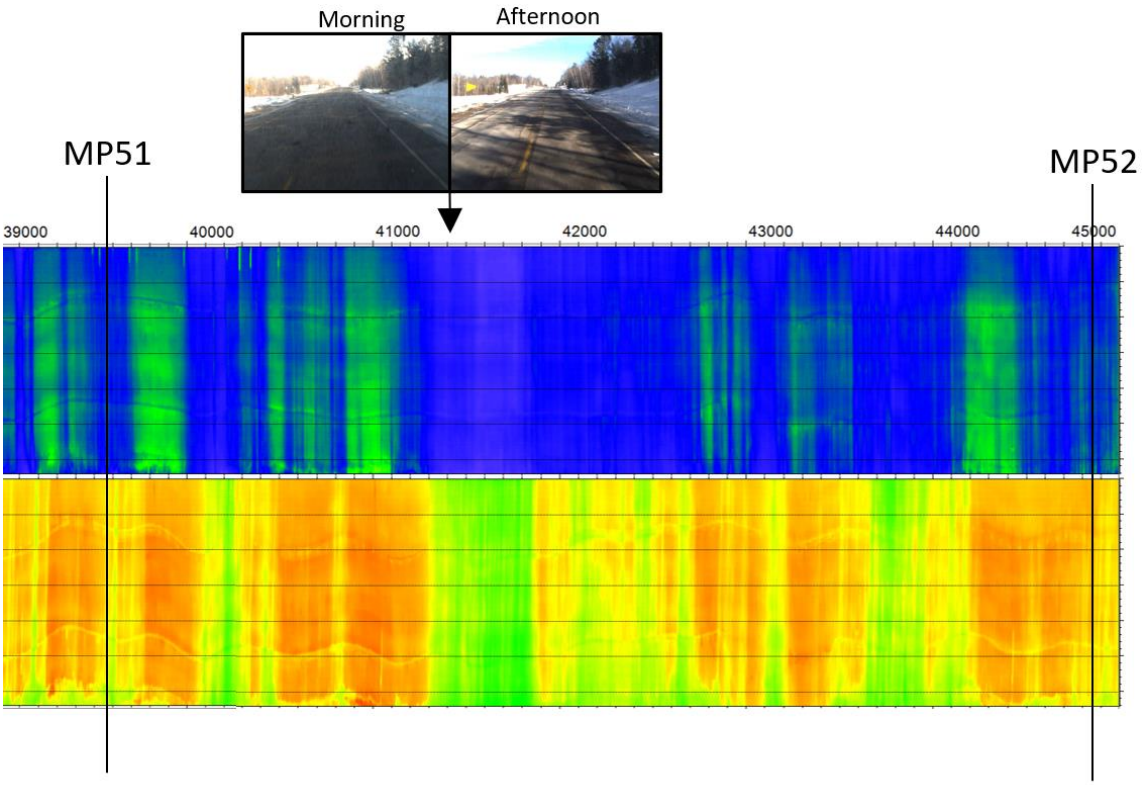

FIGURE 3. TEMPERATURE DIFFERENTIAL EFFECT OF SHADE COVER.

As shown by the heat map, there are prominent cold spots where there is significant tree shade. Using the heat map correlated with the shaded locations, test sections can be selected for point measurements of the pavement surface temperature during a later time. Tree shade factors at these points can be determined using the various methods outlined in Section 2.1. Noteworthy locations include points with no shade, intermediate amounts of shade, and complete lack of sun exposure. Using a hand-held thermal camera, measurements at the point locations at various times of the day can be made to better understand the relative effects of the tree shade on the pavement surface temperature and compare the various levels of sun exposure.

The collected climate and thermal data at the chosen locations can be used in the heat transfer model to analyze the specific conditions of the site and to perform forecasting of pavement surface temperature after selective logging and the changes in the shade factors. The development of the heat transfer model is discussed in the next chapter.

CHAPTER 4: MODELING OF HEAT TRANSFER WITH TREE AND SNOWPACK COVERS

4.1 Introduction

This chapter describes the development of the numerical heat transfer model used to predict the pavement surface temperature during winter weather on roads shaded by tree cover. The model is based on previous work done by Chadbourn et al. (1998) **[47]** and Liu et al. (2007) **[48]**. The basic elements of the model include the masses and mass fluxes of water and snow at the surface level, combined radiative and convective and latent heat fluxes at the surface level, and conductive heat fluxes through the snowpack and the pavement structure. The model is tested using MnROAD climate and thermocouple data.

4.2 The Model

A surface temperature computational model was developed based on the heat fluxes at the pavement surface. Some of the heat fluxes are dependent on the mass fluxes of snow, and water on the surface. Surface conditions are used to prescribe certain values for the thermal properties of the pavement system and properties of the snowpack. Input parameters into the model include meteorological data, which is readily available online, and pavement dimensions and material properties. The model is one-dimensional through the depth of the pavement structure. The model uses an explicit finite difference method to calculate pavement surface temperature by discretizing the depth of the pavement structure into nodes and the time frame analyzed into sufficiently small-time increments, such that the calculations satisfy the Courant-Friedrichs-Lewy (CFL) condition for stability. A two-layer system is used to model the snowpack cover on top of the pavement surface. This two-layer system is based on the model developed by Liu et al. (2007) **[48]**. The snowpack is comprised of a dry snow layer above a ‘slush’ layer. The slush layer is a porous snow matrix like that which comprises the dry snow layer, however the slush layer is saturated with liquid water. The slush layer is relatively thin and assumed to be isothermal, meaning it does not provide any insulating effect on the pavement below. An overview of the model domain is shown in Figure 4**.** Snowmelt processes involve complex mass

and heat transfer mechanisms which require phase changes and the corresponding energy gain or loss.

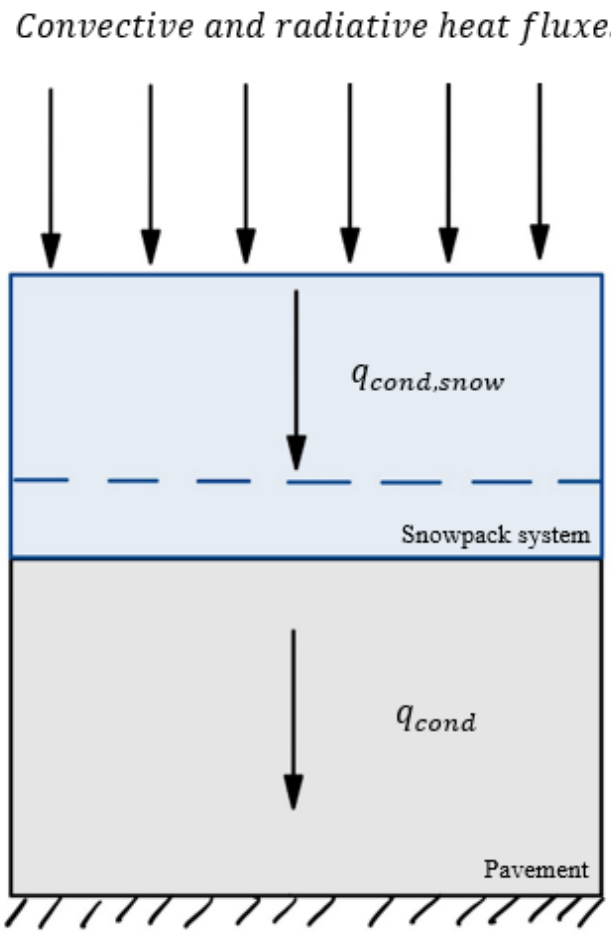

FIGURE 4. OVERVIEW OF THE MODEL DOMAIN.

4.3 Mass Balance at the Surface

When considering a snowpack cover at the pavement surface, it is important to consider the mass balance of the water. Mass fluxes of water and ice at the surface introduce heat fluxes at the pavement surface boundary. For the model, mass fluxes of water and snow/ice are considered. Mass balance of chemicals can also be included to fully consider the effects de-icing agents can

have on the heat transfer through the snowpack; however, the effects of chemicals were omitted from this simplified model.

4.3.1 Mass Balance of Water

The mass flux of water at the pavement surface (kg m^{-2} s^{-1}) is determined by summing the mass flux due to rainfall, condensation and evaporation, melting, and runoff from the surface:

$$\dot{m}_w = \dot{m}_{wp} + \dot{m_{wc}} + \dot{m}_m - \dot{m}_{wr} \quad (1)$$

The mass flux of rain, $\dot{m}_{wp}$ (kg m^{-2} s^{-1}), is a user input which can be determined readily from historic weather data. The mass flux of evaporation or condensation, $\dot{m}_{wc}$ (kg m^{-2} s^{-1}), is determined following Denby et al. (2013) **[49]**:

$$\dot{m}_{wc} = \rho_a * (SH_a - SH_s)/r_q \quad (2)$$

where ρ_a is the density of air (kg m^{-3}), SH_a and SH_s are the atmospheric and surface specific humidity, and r_q is the aerodynamic resistance for water vapor (s m^{-1}). The calculations of q_a, q_s, and r_q are shown in the Appendix. The mass flux of melting, $\dot{m}_m$ (kg m^{-2} s^{-1}), is determined by:

$$\dot{m}_m = q_{total}/L_f \quad (3)$$

where q_{total} is the total heat flux at the pavement surface (W m^{-2}) and L_f is the latent heat of fusion of water (334 kJ kg^{-1}). Melting occurs when there is snow present at the surface, the pavement temperature is at or above the melting temperature, and the total heat flux at the surface is positive; for other conditions, this flux is assumed to be zero. The melting temperature is assumed to be zero degrees Celsius. The presence of de-icing chemicals that lower the melting temperature is omitted for this model but should be considered if de-icing chemicals are present at the site. The mass flux due to runoff, $\dot{m}_{wr}$ (kg m^{-2} s^{-1}), represents the melt water that is not retained within the two-layer snow and slush system. The pavement below is assumed to be

ideally drained, so the melt water leaves instantaneously at zero degrees Celsius. A limited amount of water is retained within this two-layer system near the pavement surface. The depth of the water within the snowpack has a fixed maximum equilibrium height at which the capillary forces and gravity forces are balanced. For freshly fallen snow, this equilibrium height was found to be 2.5 centimeters by Jordan et al. (1999) **[50]**. When no snow is present, it is assumed that no water is retained on the pavement surface.

4.3.2 Mass Balance of Ice

The mass balance of ice at the pavement surface (kg m^{-2} s^{-1}) is determined by summing the mass flux due to snowfall and melting of the ice within the snowpack.

$$\dot{m}_i = \dot{m}_{ip} - \dot{m}_m \quad (4)$$

The mass flux of snow, $\dot{m}_{ip}$ (kg m^{-2} s^{-1}), is a user input which can be determined readily from historic weather data. The mass flux of melting was discussed earlier in Equation 3. Snow removal is not considered in this simplified case but can be included if the mass flux of removed snow is known.

4.4 Heat Fluxes at the Surface

Pavement temperature is affected by climactic variables and pavement thermal properties. The changes in pavement temperature are governed by several heat transfer modes; namely: conduction, convection, radiation, and latent heat fluxes **[51]**.

4.4.1 Conduction

Conduction is a heat transfer through solids caused by a difference between warm and cold sides of the solids. For a pavement system, this heat transfer occurs between the layers of the pavement system and the subgrade below. Conduction is described by the classical differential equation of Fourier's law for one-dimensional steady state **[51]**:

$$q_z = -k * \frac{\partial T}{\partial z}$$

(5)

Here k is a proportionality constant which is the thermal conductivity of the material (W m^{-1} K^{-1}), ∂z is the node distance (m), and ∂T is the temperature difference between two bodies (K). An explicit finite difference method is used to determine the pavement structure and subgrade temperature at various depths. A node distance is chosen such that the pavement and subgrade layer boundaries correspond to the boundaries between the nodes of the model. Proper weighting of the thermal properties is performed at the boundaries. Conduction following the explicit finite difference method follows the scheme as follows:

$$q_{in,_i} = q_{out,_{i-1}}$$

(6)

$$q_{out_i} = k_i * \frac{\left[T_i^{j-1} - T_{i+1}^{j-1}\right]}{dt}$$

(7)

$$T_i^j = T_i^{j-1} + \frac{1}{\left(\rho c_p\right)_i} * \frac{dt}{dz} * (q_{in} - q_{out})_i$$

(8)

Here, superscript j signifies the time step at which the calculations occur, subscript i signifies the node number, T is the temperature of a node in Celsius, dt is the time step increment (s), dz is the depth increment (m), and q_{in} and q_{out} is the flux in and out of the node (W m^{-2}), respectively.

In the presence of a dry snow cover, there is an insulation effect on the pavement below, therefore it is important to consider conduction through the dry snow layer. This conduction heat flux is:

$$q_{cond,snow} = \frac{k_{snow}}{H_{snow}}(T_{snow,top} - T_{snow,bottom})$$

(9)

Here k_{snow} is the conductivity of the dry snow layer (W m^{-1} K^{-1}), H_{snow} is the height of the dry snow layer (m), and $T_{snow,top}$ and $T_{snow,bottom}$ are the temperatures in Celsius of the top and bottom boundaries of the dry snow layer, respectively. The conductivity of snow is dependent on the density of the snow and can be empirically calculated **[52]**:

$$k_{snow} = 2.22362 + \left(\frac{\rho_{snow}}{1000}\right)^{1.885}$$

(10)

Here ρ_{snow} is the density of dry snow (kg m^{-3}). The density of snow is chosen to be 117 kg/m^3 following Jordan et al. (1999) **[50]**.

4.4.2 Convection

Convection is a heat transfer caused by a temperature difference between a flowing fluid and a solid wall. For a pavement system, this heat transfer occurs at the surface to air boundary. This process is governed by Newton's law of cooling:

$$q_{conv} = \pm h_c * (t_{b0} - t)$$

(11)

Here h_c is the heat transfer coefficient of the fluid. This simplified approach is a good estimate for most engineering applications **[51]**. This heat convection coefficient is primarily driven by wind. A discussion of empirical relationships for convection coefficients due to wind direction, characteristic length, and wind speed has been done by Palyvos (2008) **[53]**. The most used empirical equations used to estimate the convective coefficient for temperature profile prediction in pavements are the Vehrencamp **[54]**, Jurges **[55]**, and horizontal flat plate **[56]** approach models. These equations were assessed and compared by Dempsey (1970) **[54]**. The predicted temperature profiles using the different convective coefficients were compared with LTTP data, with the Vehrencamp equation achieving the highest error. Additionally, an estimate of

convection accounting for a combination of atmospheric turbulence and vehicle traffic turbulence is described by Denby et al. (2013) **[49]**. For this model, convection equation used is as described by Chadbourn et al. (1998) **[47]**:

$$q_{conv} = h_c * \left(T_{p0} - T_{amb}\right)$$

(12)

where the heat transfer coefficient is dependent on wind speed 2 meters above the pavement surface, *w* (m s^{-1}):

$$h_c = 7.4 + 6.39 * (w^{0.75})$$

(13)

4.4.3 Radiation

Radiation results from energy emitted from the sun and is divided into two forms: longwave and shortwave radiation. Longwave radiation is reflected by the gases in the atmosphere and the earth surface, and shortwave radiation comes directly from the sun **[57]**. A simplified approach for most engineering applications assumes that radiative energy flux only occurs at the surface of a body. Radiation is described by Stefan-Boltzmann's differential equation:

$$q_{LW} = \varepsilon * \sigma * (T_{body}^4 - T_{amb}^4)$$

(14)

Here ε is the emittance of the body and σ is the absorptance of the body, which is the Stefan-Boltzmann coefficient **[51]**. The ambient temperature described in the equation is the ambient sky temperature, which is estimated from the measured ambient air temperature, following Karn et al. (2019) **[58]**. The emittance of the surface at the different surface conditions is listed in Table 1. These values were obtained from Nuijten (2016) **[26]**.

TABLE 1. EMITTANCE COEFFICIENTS FOR DIFFERENT SURFACE CONDITIONS.

Condition	Surface emissivity (ε)
Dry Asphalt	0.85-0.90
Wet Asphalt	00.90-0.96
Dry Snow	0.97
Wet Snow/Slush	0.9

Solar radiation absorbed by the surface is a function of the absorptance of the pavement body, and can be estimated from the net solar flux at the top of the atmosphere:

$$q_{SW} = (1 - \alpha) * q_{SW,in} \quad \textbf{(15)}$$

Here α is the albedo of the surface, dependent on the surface condition, and $q_{SW,in}$ is the incoming solar radiation at the surface (W m^{-2}). Several methods to estimate clear-sky irradiance values exist, like one available from ASHRAE **[59]** and the one developed for use in the PaveCool model **[47]**. The surface flux for clear sky can be estimated following Schmetz (1993) **[60]**. Here, a ratio of how much radiation is blocked by cloud cover can be assumed. Similarly, shortwave radiation can be estimated existing meteorological models, such as the one described by Ashton (1986) **[61]**. Here, a quadratic formula can be used to consider the effects of cloud cover. Moreover, incident solar radiation at the surface can be measured at a weather station and the measurements can be directly used. In the absence of direct measurements, the chosen model for estimating solar heat flux at the surface for a clear sky is the empirical equation developed by Schmetz **[60]**, where the solar flux at the top of the atmosphere is calculated following the model described in the PaveCool model **[47]**. The procedure can be found in the Appendix. The empirical calculation of surface solar radiation for a clear sky is as follows:

$$q_{SW,clr} = 0.828 * q_{SW,atm} - 47.4 \frac{W}{m^2} \quad \textbf{(16)}$$

where $q_{SW,atm}$ is the clear sky flux at the top of the atmosphere (W m^{-2}). To consider cloud cover, an assumption is made that 100 percent cloud cover will block 100 percent of clear sky radiation:

$$q_{SW} = q_{SW,clr} * \left(1 - \frac{CC}{100}\right)$$

(17)

where *CC* is the percent cloud cover. To consider tree cover, a shade factor is then placed on the surface solar flux:

$$q_{SW,tree} = q_{SW} * (1 - SF)$$

(18)

where *SF* is the shade factor (between 0 and 1) determined following one of the procedures discussed in Section 2.1**.** A shade factor of 0 means no trees are present at the site, and a shade factor of 1 means all the surface solar flux is blocked by tree shade. Based on the literature review, the shade factor is realistically between 0 and 0.6.

The albedo of the surface at the different surface conditions is listed in Table 2. These values were taken from Nuijten (2016) **[26]**.

TABLE 2. ALBEDO FOR DIFFERENT SURFACE CONDITIONS.

Condition	Albedo (α)
Dry Asphalt	0.10-0.15
Wet Asphalt	0.10-0.20
Dry Snow	0.6
Wet Snow/Slush	0.3-0.6

4.4.5 Precipitation

Heat fluxes due to snowfall and rainfall are modeled following Liu et al. (2007) **[48]**. The heat transfer follows the relationships:

$$q_{rain} = \dot{m}_{wp} * c_{pw} * \left(T_{amb} - T_{p0}\right)$$

(19)

$$q_{snow} = \dot{m}_{ip} * c_{ps} * \left(T_{amb} - T_{p0}\right)$$

(20)

Where c_{pw} and c_{ps} are the specific heat capacities of water and snow (J kg^{-2} K^{-1}), respectively.

4.4.6 Latent Heat Flux

Heat fluxes due to evaporation and condensation (W m^{-2}) follow the relationship:

$$q_{evap/cond} = L_v * \dot{m}_{wc}$$

(21)

where L_v is the latent heat of vaporization for water (J kg^{-1}). If the surface temperature is above the melting temperature and below the dew point, condensation occurs. If the surface temperature is above the melting temperature and above the dew point, evaporation occurs. The approximate dew point temperature is calculated according to a proposed relationship by Lawrence (2005) **[62]**:

$$T_d = T - \frac{100 - RH}{5}$$

(22)

where T is the air temperature in Celsius and RH is the relative humidity, which can be obtained from historic weather data or measured. This relationship is fairly accurate for relative humidity values above 50 percent, which is a fair assumption for the humidity conditions in Minnesota. If evaporation occurs, energy is added to the total heat flux at the pavement surface. If condensation occurs, energy is subtracted from the total heat flux at the pavement surface.

The heat lost due to melting the snowpack (W m^{-2}) is subtracted from the total incoming heat flux at the surface. This lost heat is calculated as follows:

$$q_{melt} = \dot{m}_m * L_f$$

(23)

The pavement surface temperature is maintained at 0 degrees Celsius for the duration of the melting.

4.4.7 Heat fluxes due to Traffic

Vehicle traffic can introduce a lot of sensible heat to the pavement **[63]**. For the model, heat fluxes due to vehicle traffic are omitted under the assumption that the road segment examined will have low amounts of vehicle traffic. For sites with a lot of vehicle traffic, the heat fluxes due to traffic should be included.

4.5 Model Input Data

Validation for the model was performed using measured meteorological and thermocouple data and pavement properties for test sections 15-D-2004 and 1-D-2006/2012 at the MnDOT MnROAD facility. The testing facility is located 45° 15' 36.9714", -93° 42' 7.1634" at an altitude of 294 meters. The pavement structure of test section 15-D-2004 consists of an 11.1-inch hot-mix asphalt layer with 2 layers of microsurfacing on a clay subgrade. The specifics of the layer structure are shown in Figure 5. The pavement structure of test section 1-D-2006/2012 consists of a 6-inch hot-mix asphalt layer on a 33-inch gravel base. These two layers sit on a clay subgrade. The specifics of the layer structure are shown in Figure 6.

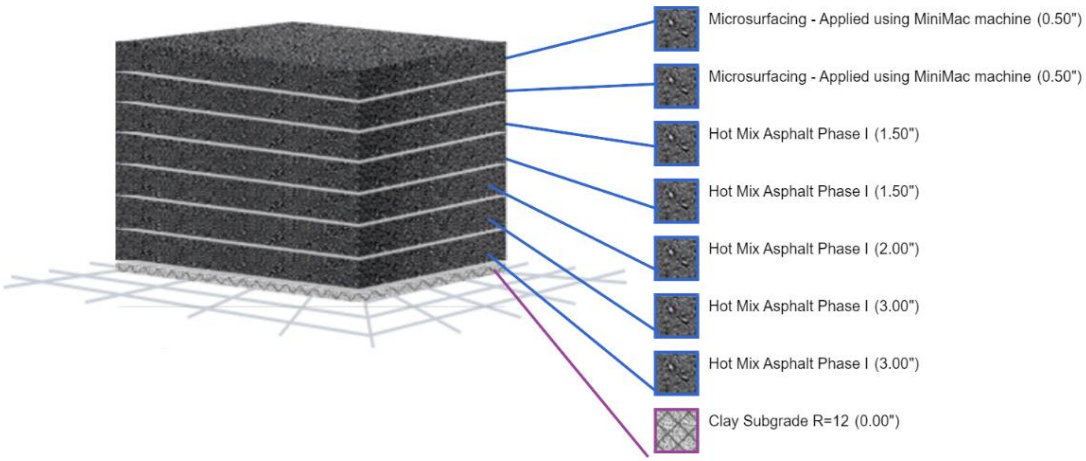

FIGURE 5. LAYER STRUCTURE FOR TEST SECTION 15-D-2004.

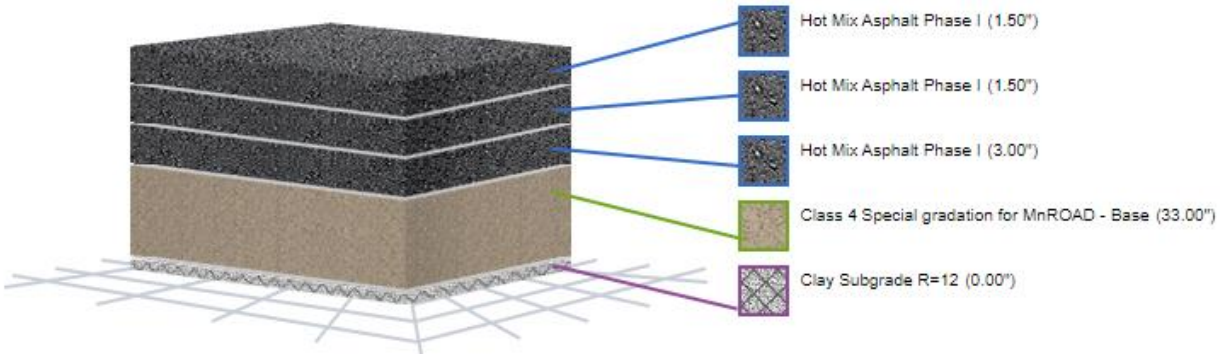

FIGURE 6. LAYER STRUCTURE FOR TEST SECTION 1-D-20062012.

The meteorological data used as input for the site includes precipitation intensity (0.01 in), relative humidity (%), atmospheric pressure (mbar), air temperature (Celsius), wind speed (m/s), and total surface solar flux (W/m2). No estimates were necessary for the shortwave radiation heat flux given the total surface solar flux data was collected at the weather station. This information was collected at the MnROAD site weather station. Climate data is collected every quarter hour. Similarly, thermocouple data was extracted from the sensor database. The thermocouple data is also collected every quarter hour. The thermocouple sensors used were located between 0.03 and 2.45 meters below the pavement surface.

The model was tested using two time periods. A 10-hour period on January 25, 2004, was used to test the model and investigate the various sub-models. This 10-hour period between 00:00 and 10:00 contains minimal precipitation and occurred after a snow event the previous day. A node distance of 0.02 meters and a time step of 3 minutes was selected to satisfy the CFL stability condition. Given the climate data was collected at 15-minute intervals, an assumption was made that those measurements were valid for the entire period to match the temporal frequency. A 1-inch dry snow cover was assumed to test the conduction flux through the snowpack. This assumption was made from the historic daily snow depth for the area. An initial thermal curve within the pavement structure was assumed by using known thermocouple data at the start of the analysis period. Linear interpolation was used to estimate the temperature between the thermocouple locations. The pavement structure used for this analysis was that of test cell 15-D-2004.

A 6-month period from September 01, 2011, to April 30, 2012, was used to test the model for a longer time frame with more variability in weather conditions. A node distance of 0.05 meters and a time step of 15 minutes was selected to satisfy the CFL stability condition. The climate data for this period didn't contain measurements of average wind speed. Random values for wind speed were generated using the Rayleigh distribution using historic mean wind speeds for each month. Rayleigh distribution was selected because of its use to model wind energy potential **[64]**. An initial thermal curve within the pavement structure was assumed by using the same method as for the first analysis. The pavement structure used for this analysis was that of test cell 1-D-2006/2012.

CHAPTER 5: RESULTS

5.1 Sensitivity Analysis

Using data for the 10-hour period, the sensitivity of several input variables was tested. Several values for conductivity and heat capacity of the asphalt and clay subgrade were tested at different values to test their effects on the pavement surface temperature. The calculated temperature was compared to the measured data of the thermocouple closest to the pavement surface, at 0.03 meters below the surface. The average error and root-mean-square-error (RMSE) results for each case are shown in Table 3. Best case scenario is shown in the first row, with the other rows showing how the result varied by changing one parameter from the best case. The other cases for run but are not shown in the table. The thermal properties resulting in the best case were used.

TABLE 3. SENSITIVITY ANALYSIS RESULTS FOR INPUT THERMAL PROPERTY VALUES.

$k_{asphalt}$ [W m^{-1} K^{-1}]		k_{clay} [W m^{-1} K^{-1}]		$C_{p,asphalt}$ [J kg^{-1} K^{-1}]		$C_{p,clay}$ [J kg^{-1} K^{-1}]		Average Error [%]	RMSE [Celsius]
0.76	1.21	0.15	1	850	920	878	1381		
	x	x			x	x		1.525	0.1525
x		x			x	x		2.018	0.2209
	x		x		x	x		-1.8	0.2111
	x	x		x		x		1.684	0.1974
	x	x			x		x	1.669	0.1933

The radiative, convective, and precipitative heat fluxes at the surface were calculated using the model and plotted to verify if the fluxes make sense physically. These fluxes are shown in Figure 7. The latent heat fluxes due to rain and snow are very small which is accurate as the precipitation during the 10-hour analysis period was minimal; only small amounts of snowfall occurred. The shortwave radiation heat flux was close to zero and started gradually increasing starting at 8:00 am.

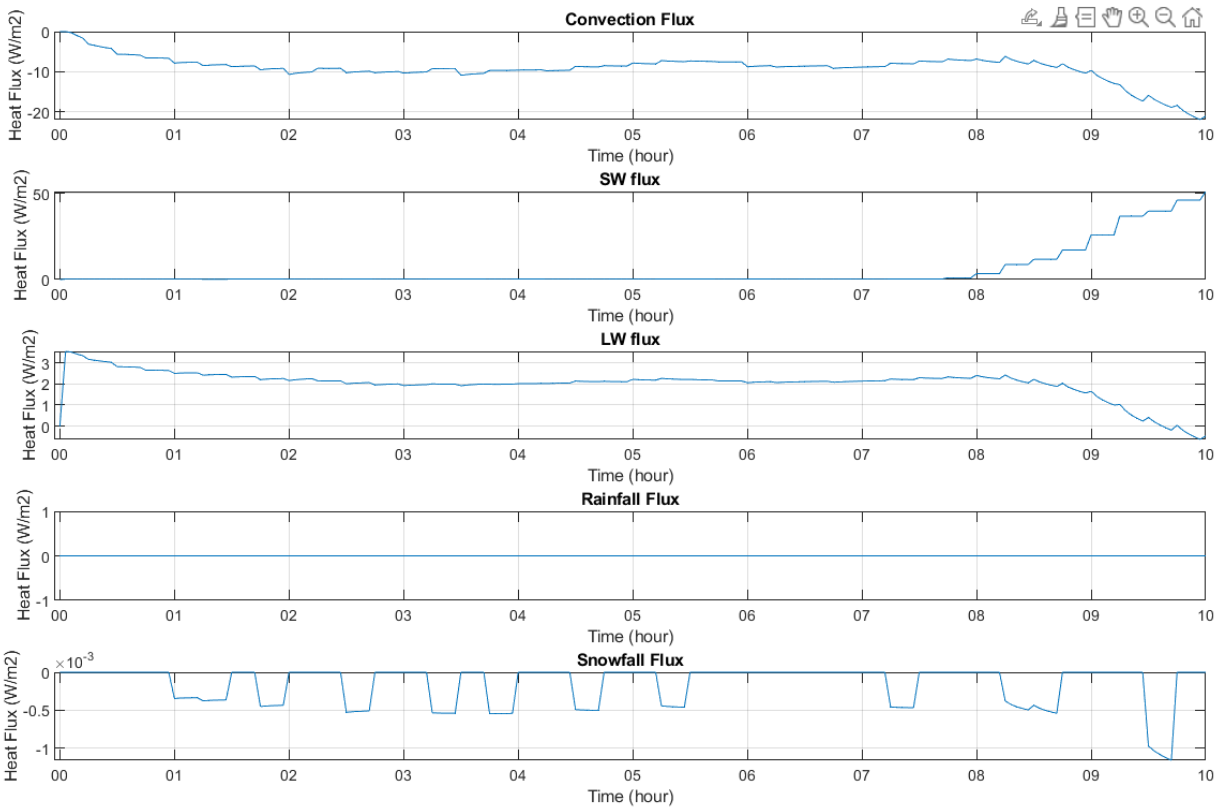

FIGURE 7. THE CONVECTION, SHORTWAVE RADIATION, LONGWAVE RADIATION, RAINFALL, AND SNOWFALL HEAT FLUXES DURING THE 10-HOUR PERIOD ON JANUARY 25, 2004, 00:00 TO 10:00.

The pavement calculated temperature compared to the measurements of the thermocouple closest to the pavement surface are shown in Figure 8. The average error for the data was 1.53% and the RMSE of the data was 0.1525 degrees Celsius. These results show that the model predicts the temperature well compared to the measured temperature.

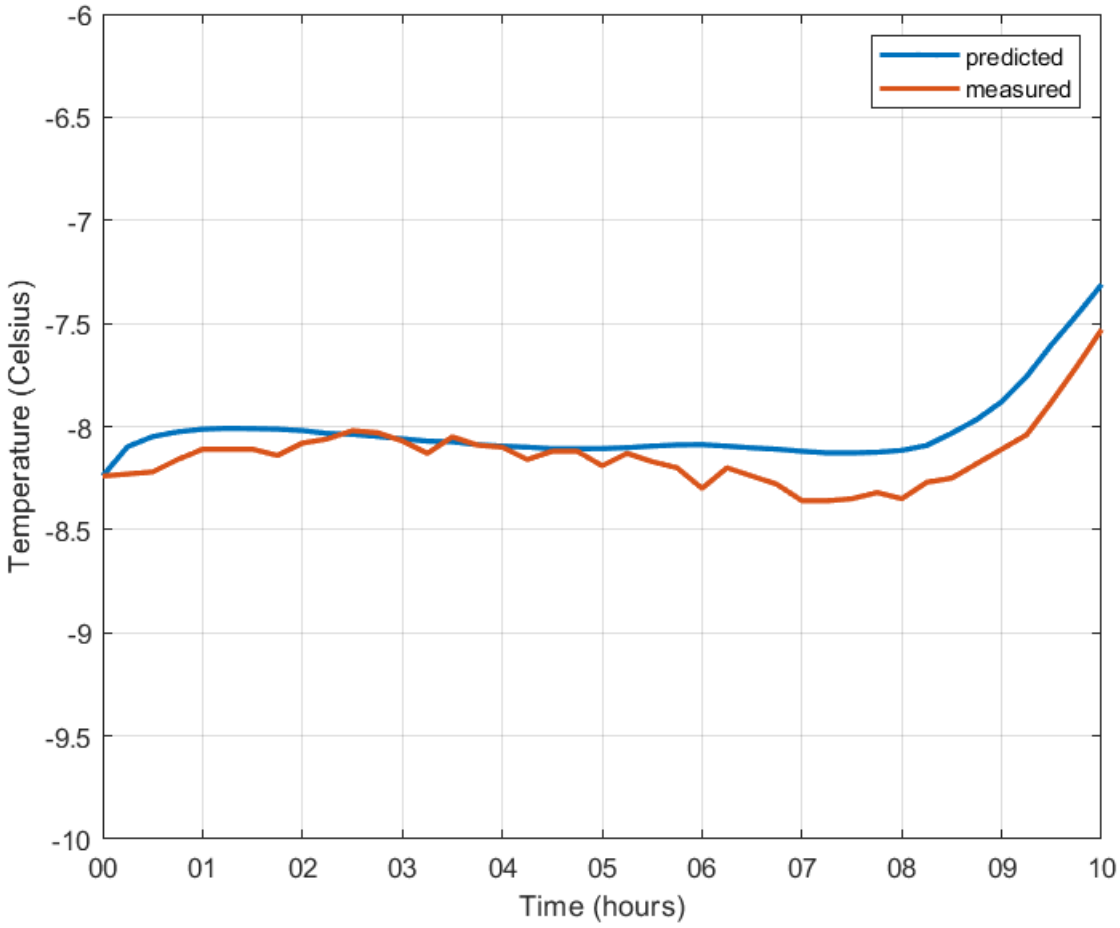

FIGURE 8. PREDICTED AND MEASURED TEMPERATURE AT A DEPTH OF 0.03 METERS BELOW PAVEMENT SURFACE.

5.2 Long-Term Prediction Results

The 6-month period was analyzed to include variability in weather conditions and effects of snowmelt. The closest depth to surface that had thermocouple data available was 0.1250 meters. The pavement calculated temperature compared to the measurements of the thermocouple closest to the pavement surface are shown in Figure 9. The average error for the data was 8.32% and the RMSE of the data was 1.544 degrees Celsius. These are larger errors; however, when isolating the data for the winter months of November to March when the pavement temperature is the coldest, average error for the data was 4.06% and the RMSE of the data was 1.116 degrees Celsius.

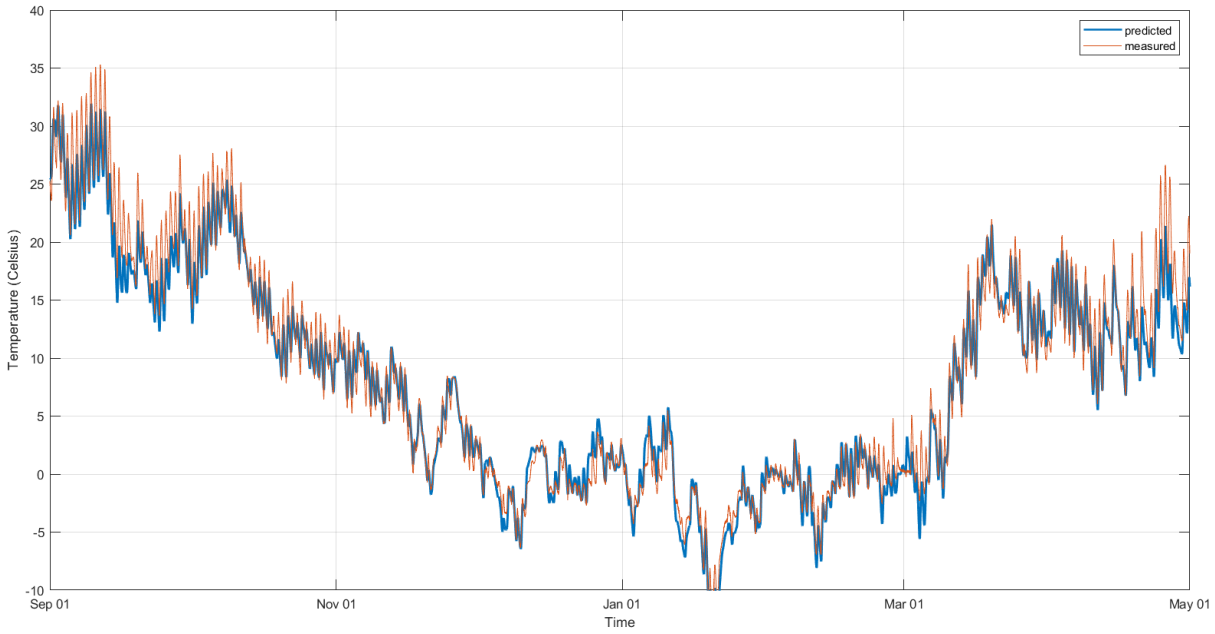

FIGURE 9. PREDICTED AND MEASURED PAVEMENT TEMPERATURE AT A DEPTH OF 0.1250 METERS FOR WINTER SEASON OF 2011-2012.

5.3 Shade Factor Effects

A sample analysis was performed considering various shade factors for the 6-month analysis period. The model was run considering varying degrees of shade, and the total number of hours within the 6-month period where the pavement temperature dropped below -9.4 Celsius. This limiting temperature is the point at which deicers are considered no longer effective. The percentage of hours during which the temperature is below the limit plotted against the shade factor is shown in Figure 10.

The percentage of time that the surface temperature is below the de-icing effectiveness limit is very small, on the scale of 0.1%, but this is also considering the entire time of the winter season; a more accurate assumption would be to consider specific snowfall events when there would be snow present on the pavement surface and the use of deicers would be considered.

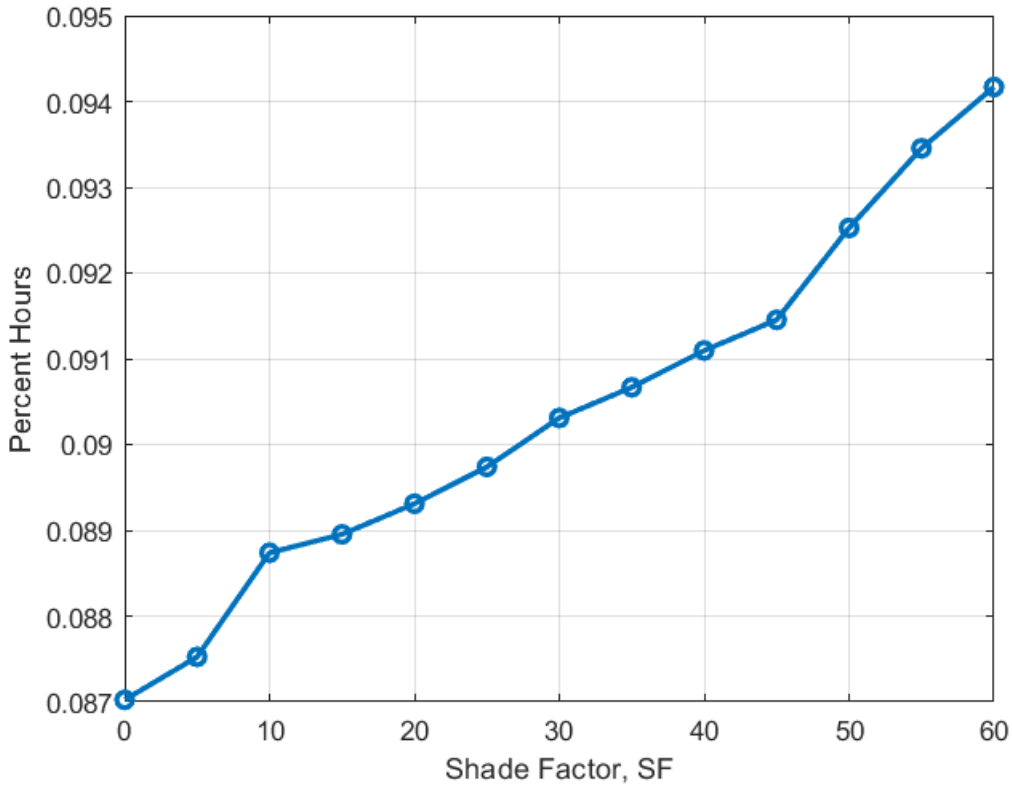

FIGURE 10. PERCENTAGE OF HOURS DURING THE 6-MONTH ANALYSIS PERIOD DURING WHICH THE PAVEMENT SURFACE TEMPERATURE IS BELOW -9.4 DEGREES CELSIUS.

CHAPTER 6: CONCLUSIONS AND RECOMMENDATIONS

A numerical model to predict the surface temperature of a pavement system is developed. This model can be used to predict the effect of various amounts of tree shade on the surface temperature of a pavement below a snowpack over time. Being able to accurately predict the surface temperature can be a helpful tool in determining the balance between amount of sun exposure and necessary surface temperature for effective de-icing of the road surface for winter maintenance.

The developed model performed well for a 10-hour period during which there was minimal precipitation and a relatively thin snowpack consisting of dry snow. The average error between the measured thermocouple data and the predicted data was 1.525% and the RMSE was 0.1525. The model performed less well for the 6-month period. The average error between the measured and predicted data was 8.32% with an RMSE of 1.544. The error was reduced to 4.06% with an RMSE of 1.116 when only winter months where the surface temperature was coldest were considered. A test was done for the 6-month period to assess the influence of the shade factor on the pavement surface temperature. The total time during which the surface temperature was below the deicing effectiveness temperature limit of -9.4 degrees Celsius was on the order of 0.1% for shade factors between 0 and 0.6; however, this was considering the entire 6-month period. It is recommended to explore specific snowfall events to assess the effects of the shade factor. The model's performance is dependent on the accuracy of the weather data and the accuracy of the pavement structure properties. The model was tested with MnROAD data, which was not checked for accuracy. Assumptions for the pavement and subgrade thermal properties could have also influenced the model performance. More calibration and validation of the model should be performed.

Future recommendations for the project include determining viable test point locations for the TH34 road segment with variable sun exposure levels using Road Doctor data. One of the techniques for measuring shade factors can be used to determine the levels of shade at the test points. This should be done during the wintertime when the deciduous trees are in the "leafless"

condition. Hand-held thermal camera imagery can be used to compare the relative effects of differing tree shade amounts throughout the day. Collection of climate and thermal data for snow events at these points which can be used in the heat transfer model will be useful in determining how much selective tree removal to consider.

REFERENCES

[1] Asaeda, T., Ca, V. T., & Wake, A. (1996). Heat storage of pavement and its effect on the lower atmosphere. *Atmospheric Environment*, *30*(3), 413–427. https://doi.org/10.1016/1352-2310(94)00140-5

[2] Rahman, M. A., Armson, D., & Ennos, A. R. (2014). A comparison of the growth and cooling effectiveness of five commonly planted urban tree species. *Urban Ecosystems*, *18*(2), 371–389. https://doi.org/10.1007/s11252-014-0407-7

[3] Li, H. (2016). Introduction. *Pavement Materials for Heat Island Mitigation*, 1–13. https://doi.org/10.1016/b978-0-12-803476-7.00001-5

[4] Napoli, M., Massetti, L., Brandani, G., Petralli, M., & Orlandini, S. (2016). Modeling Tree Shade effect on urban ground surface temperature. *Journal of Environmental Quality*, *45*(1), 146–156. https://doi.org/10.2134/jeq2015.02.0097

[5] Liu, B. Y. H., & Jordan, R. C. (1960). The Interrelationship and characteristic distribution of direct, diffuse and total solar radiation. *Solar Energy*, *4*(3), 1–19. https://doi.org/10.1016/0038-092x(60)90062-1

[6] Youngberg, R. (1983). Shading effects of deciduous trees. *Arboriculture & Urban Forestry*, *9*(11), 295–297. https://doi.org/10.48044/jauf.1983.069

[7] Yates, D., & McKennan, G. (1989). Solar architecture and light attenuation by trees: Conflict or compromise? *Arboricultural Journal*, *13*(1), 7–16. https://doi.org/10.1080/03071375.1989.9756396

[8] Wagar, J. A., & Heisler, G. M. (1986). Rating Winter Crown density of deciduous trees: A photographic procedure. *Landscape Journal*, *5*(1), 9–18. https://doi.org/10.3368/lj.5.1.9

[9] Kumakura, E., Nakaohkubo, K., & Hoyano, A. (2013). Solar Shading Effects by Tree Species in an Urban Environment Using Numerical Simulation Tool.

[10] Gardner, T. J., & Sydnor, T. D. (1984). Interception of summer and winter insolation by five shade tree species. *Journal of the American Society for Horticultural Science*, *109*(4), 448–450. https://doi.org/10.21273/jashs.109.4.448

[11] Heisler, G. M. (1986). Effects of individual trees on the solar radiation climate of small buildings. *Urban Ecology*, *9*(3-4), 337–359. https://doi.org/10.1016/0304-4009(86)90008-2

[12] Lotufo Bueno-Bartholomei, C. & Labaki, L. (2003). How much does the change of species of trees affect their solar radiation attenuation. *Int. Conf. Urban Clim.. 5. 267-270.*

[13] Konarska, J., Lindberg, F., Larsson, A., Thorsson, S., & Holmer, B. (2013). Transmissivity of solar radiation through crowns of single urban trees—application for outdoor thermal comfort modelling. *Theoretical and Applied Climatology*, *117*(3-4), 363–376. https://doi.org/10.1007/s00704-013-1000-3

[14] McPherson, E. G., Xiao, Q., van Doorn, N. S., Johnson, N., Albers, S., & Peper, P. J. (2018). Shade factors for 149 taxa of in-leaf urban trees in the USA. *Urban Forestry & Urban Greening*, *31*, 204–211. https://doi.org/10.1016/j.ufug.2018.03.001

[15] Tan, P. Y., Wong, N. H., Tan, C. L., Jusuf, S. K., Chang, M. F., & Chiam, Z. Q. (2018). A method to partition the relative effects of evaporative cooling and shading on air temperature within vegetation canopy. *Journal of Urban Ecology*, *4*(1). https://doi.org/10.1093/jue/juy012

[16] Rahman, M. A., Moser, A., Rötzer, T., & Pauleit, S. (2019). Comparing the transpirational and shading effects of two contrasting urban tree species. *Urban Ecosystems*, *22*(4), 683–697. https://doi.org/10.1007/s11252-019-00853-x 3585 3605

[17] Trenberth, K. E., Fasullo, J. T., & Kiehl, J. (2009). Earth's Global Energy Budget. *Bulletin of the American Meteorological Society*, *90*(3), 311–324. https://doi.org/10.1175/2008bams2634.1

[18] Lilek, J. (2017, July). Roadway deicing in the United States. American Geosciences Institute.

[19] Klein-Paste, A., & Potapova, J. (2014). Thermal aspects of melting ice with Deicer Chemicals. *Transportation Research Record: Journal of the Transportation Research Board*, *2440*(1), 69–75. https://doi.org/10.3141/2440-09

[20] Laurinavičius, A., Čygas, D., Vaitkus, A., Ratkevičius, T., Bulevičius, M., Mučinis, D., & Baltrušaitis, A. (2016). Research of snow melting materials performance efficiency for road winter maintenance. *TRANSPORT, 31*(3), 322–332. https://doi.org/10.3846/16484142.2016.1211551

[21] Minnesota Department of Transportation. (2012). Minnesota Snow and Ice Control. Minnesota Local Road Research Board (LRRB). https://www.dot.state.mn.us/maintenance/manual.html

[22] Li, Y., Fang, Y., Seeley, N., Jungwirth, S., Jackson, E., & Shi, X. (2013). Corrosion by chloride deicers on highway maintenance equipment. *Transportation Research Record: Journal of the Transportation Research Board*, *2361*(1), 106–113. https://doi.org/10.3141/2361-13

[23] Xie, N., Shi, X., & Zhang, Y. (2017). Impacts of potassium acetate and sodium-chloride deicers on concrete. *Journal of Materials in Civil Engineering*, *29*(3). https://doi.org/10.1061/(asce)mt.1943-5533.0001754

[24] Fay, L., & Shi, X. (2012). Environmental impacts of chemicals for snow and ice control: State of the knowledge. *Water, Air, & Soil Pollution*, *223*(5), 2751–2770. https://doi.org/10.1007/s11270-011-1064-6

[25] Chapin, F., Omitaomu, O., & Bhaduri, B. L. (2017). Making roads safer: Optimizing de-icing using snowmelt rates and slope data. *Proceedings of the 2nd World Congress on Civil, Structural, and Environmental Engineering*. https://doi.org/10.11159/icte17.104

[26] Nuijten, A. D. W. (2016). Runway temperature prediction, a case study for Oslo Airport, Norway. *Cold Regions Science and Technology*, *125*, 72–84. https://doi.org/10.1016/j.coldregions.2016.02.004

[27] Shao, J., & Lister, P. J. (1996). An automated nowcasting model of road surface temperature and state for Winter Road Maintenance. *Journal of Applied Meteorology*, *35*(8), 1352–1361. https://doi.org/10.1175/1520-0450(1996)035<1352:aanmor>2.0.co;2

[28] Chen, J., Wang, H., & Xie, P. (2019). Pavement temperature prediction: Theoretical models and critical affecting factors. *Applied Thermal Engineering*, *158*, 113755. https://doi.org/10.1016/j.applthermaleng.2019.113755

[29] Bogren, J., Gustavsson, T., Karlsson, M., & Postgård, U. (2000). The impact of screening on road surface temperature. *Meteorological Applications*, *7*(2), 97–104. https://doi.org/10.1017/s135048270000150x

[30] Middel, A., Lukasczyk, J., & Maciejewski, R. (2017). Sky view factors from synthetic fisheye photos for thermal comfort routing—a case study in Phoenix, Arizona. *Urban Planning*, *2*(1), 19–30. https://doi.org/10.17645/up.v2i1.855

[31] Karsisto, V., & Horttanainen, M. (2023). Sky View Factor and screening impacts on the forecast accuracy of road surface temperatures in Finland. *Journal of Applied Meteorology and Climatology*, *62*(2), 121–138. https://doi.org/10.1175/jamc-d-22-0026.1

[32] Dingman, S. L. (2015). Snow and Snowmelt. In *Physical Hydrology* (3rd ed., pp. 203–252). Waveland Press, Inc.

[33] Jordan, R.E. (1991). A One-dimensional temperature model for a snow cover: technical documentation for SNTHERM.89.

[34] Anderson, E. (2006). Snow Accumulation and Ablation Model -- SNOW-17.

[35] Golden, J. S. (2004). The built environment induced urban heat island effect in rapidly urbanizing arid regions – a sustainable urban engineering complexity. *Environmental Sciences*, *1*(4), 321–349. https://doi.org/10.1080/15693430412331291698

[36] Golden, J. S., & Kaloush, K. E. (2006). Mesoscale and microscale evaluation of surface pavement impacts on the urban heat island effects. *International Journal of Pavement Engineering*, *7*(1), 37–52. https://doi.org/10.1080/10298430500505325

[37] McPherson, E. G., & Muchnick, J. (2005). Effects of street tree shade on asphalt concrete pavement performance. *Arboriculture & Urban Forestry*, *31*(6), 303–310. https://doi.org/10.48044/jauf.2005.039

[38] Rahman, M. A., Stratopoulos, L. M. F., Moser-Reischl, A., Zölch, T., Häberle, K.-H., Rötzer, T., Pretzsch, H., & Pauleit, S. (2020). Traits of trees for cooling urban heat islands: A meta-analysis. *Building and Environment*, *170*, 106606. https://doi.org/10.1016/j.buildenv.2019.106606

[39] Santamouris, M. (2013). Using cool pavements as a mitigation strategy to fight urban heat island—a review of the actual developments. *Renewable and Sustainable Energy Reviews*, *26*, 224–240. https://doi.org/10.1016/j.rser.2013.05.047

[40] Jiang, L., Wang, L., & Wang, S. (2019). A novel solar reflective coating with functional gradient multilayer structure for cooling asphalt pavements. *Construction and Building Materials*, *210*, 13–21. https://doi.org/10.1016/j.conbuildmat.2019.03.180

[41] Iwama, M., Yoshinaka, T., Nishioka, S., & Murakami, H. (2019). Reflectivity and durability assessment of solar heat-blocking pavement. *Lecture Notes in Civil Engineering*, 133–143. https://doi.org/10.1007/978-3-030-29779-4_13

[42] Kuai, C., Chen, J., Shi, X., & Grasley, Z. (2021). Regulating porous asphalt concrete temperature using PEG/SIO2 phase change composite: Experiment and simulation. *Construction and Building Materials*, *273*, 122043. https://doi.org/10.1016/j.conbuildmat.2020.122043

[43] Pomerantz, M., Akbari, H., Chen, A., Taha, H., & Rosenfeld, A. H. (1997). Paving materials for Heat Island mitigation. https://doi.org/10.2172/291033

[44] Jiang, L., & Wang, S. (2020). Enhancing heat release of asphalt pavement by a gradient heat conduction channel. *Construction and Building Materials*, *230*, 117018. https://doi.org/10.1016/j.conbuildmat.2019.117018

[45] Jiang, L., Wang, S., Gu, X., Dorjee, N., & Bo, W. (2021). Inducing directional heat transfer by enhancing directional thermal conductivity of asphalt mixtures for improving asphalt solar collectors. *Construction and Building Materials*, *267*, 121731. https://doi.org/10.1016/j.conbuildmat.2020.121731

[46] Federal Highway Administration. (n.d.). *MnROAD Data*. LTPP InfoPave. https://infopave.fhwa.dot.gov/MnRoad/Index

[47] Chadbourn, Bruce A.; Newcomb, David E.; Voller, Vaughan R.; DeSombre, Rachel A.; Luoma, James A.; Timm, David H.. (1998). An Asphalt Paving Tool for Adverse Conditions. Retrieved from the University of Minnesota Digital Conservancy, https://hdl.handle.net/11299/1035.

[48] Liu, X., Rees, S. J., & Spitler, J. D. (2007). Modeling snow melting on heated pavement surfaces. part I: Model development. *Applied Thermal Engineering*, *27*(5–6), 1115–1124. https://doi.org/10.1016/j.applthermaleng.2006.06.017

[49] Denby, B. R., Sundvor, I., Johansson, C., Pirjola, L., Ketzel, M., Norman, M., Kupiainen, K., Gustafsson, M., Blomqvist, G., Kauhaniemi, M., & Omstedt, G. (2013). A coupled road dust and surface moisture model to predict non-exhaust road traffic induced particle emissions (NORTRIP). part 2: Surface moisture and salt impact modelling. Atmospheric Environment, 81, 485–503. https://doi.org/10.1016/j.atmosenv.2013.09.003

[50] Jordan, R. E., Hardy, J. P., Perron, F. E., & Fisk, D. J. (1999). Air permeability and capillary rise as measures of the pore structure of snow: An experimental and theoretical study. *Hydrological Processes*, *13*(12–13), 1733–1753. https://doi.org/10.1002/(sici)1099-1085(199909)13:12/13<1733::aid-hyp863>3.0.co;2-2

[51] Annaratone, D. (2009). Introduction to heat transfer. *Engineering Heat Transfer*, 1–11. https://doi.org/10.1007/978-3-642-03932-4_1

[52] Y. Yen, Review of thermal properties of snow, ice and sea ice, US Army Cold Regions Research & Engineering Laboratory Report 81 (10), 1981.

[53] Palyvos, J. A. (2008). A survey of wind convection coefficient correlations for building envelope energy systems' modeling. Applied Thermal Engineering, 28(8-9), 801–808. https://doi.org/10.1016/j.applthermaleng.2007.12.005

[54] Dempsey, B. J. (1970). A Heat-transfer Model For Evaluating Frost Action And Temperature Related Effects In Multilayered Pavement Systems (Order No. 7013289). Available from Dissertations & Theses @ CIC Institutions; ProQuest Dissertations & Theses Global. (287952616).

[55] Bentz, D. P., (2000). A Computer Model to Predict the Surface Temperature and Time-of-Wetness of Concrete Pavements and Bridge Decks. NISTIR 6551. U.S. Department of Commerce. https://tsapps.nist.gov/publication/get_pdf.cfm?pub_id=860286

[56] Chiasson, A. D., Spitler, J. D., Rees, S. J., & Smith, M. D. (2000). A model for simulating the performance of a pavement heating system as a supplemental heat rejecter with closed-

loop ground-source heat pump systems. *Journal of Solar Energy Engineering*, *122*(4), 183–191. https://doi.org/10.1115/1.1330725

[57] Klassen, S., & Bugbee, B. (2015). Shortwave radiation. *Agronomy Monographs*, 43–57. https://doi.org/10.2134/agronmonogr47.c3

[58] Karn, A., Chintala, V., & Kumar, S. (2019). An investigation into sky temperature estimation, its variation, and significance in heat transfer calculations of solar cookers. *Heat Transfer-Asian Research*, *48*(5), 1830–1856. https://doi.org/10.1002/htj.21459

[59] American Society of Heating, Refrigerating and Air-Conditioning Engineers, Inc. (ASHRAE). (2021). 2021 ASHRAE® Handbook - Fundamentals (SI Edition) - 14.3.1 Solar Angles Related to Receiving Surfaces. American Society of Heating, Refrigerating and Air-Conditioning Engineers, Inc. (ASHRAE). Retrieved from https://app.knovel.com/hotlink/pdf/id:kt012MGY3L/ashrae-handbook-fundamentals/solar-angles-related

[60] Schmetz, J. (1993). Relationship between solar net radiative fluxes at the top of the atmosphere and at the surface. *Journal of the Atmospheric Sciences*, *50*(8), 1122–1132. https://doi.org/10.1175/1520-0469(1993)050<1122:rbsnrf>2.0.co;2

[61] Ashton, G.D., 1986. River and Lake Ice Engineering. Water Resources Publications, LLC, Colorado.

[62] Lawrence, M. G. (2005). The relationship between relative humidity and the dewpoint temperature in moist air: A simple conversion and applications. *Bulletin of the American Meteorological Society*, *86*(2), 225–234. https://doi.org/10.1175/bams-86-2-225

[63] Hoehne, C. G., Chester, M. V., Sailor, D. J., & King, D. A. (2020). Urban heat implications from parking, roads, and cars: A case study of metro phoenix. *Sustainable and Resilient Infrastructure*, *7*(4), 272–290. https://doi.org/10.1080/23789689.2020.1773013

[64] Bidaoui, H., Abbassi, I. E., Bouardi, A. E., & Darcherif, A. (2019). Wind speed data analysis using Weibull and Rayleigh distribution functions, case study: Five cities northern morocco. *Procedia Manufacturing*, *32*, 786–793. https://doi.org/10.1016/j.promfg.2019.02.286

[65] Bolton, D. (1980). The computation of equivalent potential temperature. *Monthly Weather Review*, *108*(7), 1046–1053. https://doi.org/10.1175/1520-0493(1980)108<1046:tcoept>2.0.co;2

APPENDIX: ENVIRONMENTAL MODEL CALCULATIONS

Atmospheric and Surface Humidity

Calculation of atmospheric and surface specific humidities were based on Bolton (1980) **[65]**.

The saturated vapor pressure is calculated as:

$$e_s = 6.112 * \exp\left(\frac{17.67 * T}{T + 243.5}\right) \quad \textbf{(24)}$$

where:

T is ambient air temperature (Celsius)

The vapor pressure is then determined from the relative humidity measurements:

$$e = e_s * \left(\frac{RH}{100}\right) \quad \textbf{(25)}$$

The surface specific humidity is calculated as:

$$SH_s = \frac{0.622 * e}{p - 0.378 * e} \quad \textbf{(26)}$$

where:

p is the measured atmospheric pressure at the surface (mbar)

The atmospheric specific humidity is calculated as:

$$SH_a = \frac{0.622 * e}{(e_s - e)} \quad \textbf{(27)}$$

Aerodynamic resistance for water vapor

Calculation of the aerodynamic resistance for water vapor, r^q (s m^{-1}), is:

$$r_q = \frac{\ln\left[\frac{z_m - d}{z_{om}}\right] \ln\left[\frac{z_h - d}{z_{oh}}\right]}{\kappa^2 u_z} \quad \textbf{(28)}$$

where:

z_m is height of wind measurements (m)

z_h is height of of humidity measurements (m)

d is zero plane displacement height (m)

z_{om} is roughness length governing momentum transfer (m)

z_{oh} is roughness length governing transfer of heat and vapor (m)

κ is von Karman's constant, 0.41

u_z is wind speed at height z (m s^{-1})

Making assumptions that d = 0 meters for bare ground, $z_h = z_m = 2$ meters, and that $z_{oh} = 0.1 z_{om}$. A value of 0.01 meters was chosen for the roughness lengths for momentum.

Calculation of net solar flux at the top of the atmosphere

In absence of total incident shortwave radiation measurements, the net solar flux on a pavement surface can be estimated following the procedure outlined in the PaveCool model **[47]**. The solar flux at the top of the atmosphere is dependent on the location of the site, day of the year, and the time of the day. The procedure is as follows:

1. To calculate the earth's angular displacement from the major axis of orbit, θ (radians):

$$\theta = 2\pi * \frac{d-2}{365.242} \qquad 365 \leq d \leq 2$$

(29)

$$\theta = 2\pi * \frac{d+363}{365.242} \qquad 1 \leq d \leq 2$$

(30)

2. To calculate the angular fraction of a year represented by day number, ψ (radians):

$$\psi = 2\pi * \frac{d-1}{365.42}$$

(31)

3. To calculate the solar declination, D (radians):

$$D = \sin^{-1}[\sin(0.409172) * \sin\sigma]$$

(32)

where:

$$\sigma = 4.885784 + 3.342004 \times 10^{-2} * \sin(\psi) - 1.3880 \times 10^{-3} * \cos(\psi)$$
$$+3.4798 \times 10^{-4} \sin(2\psi) - 2.285 \times 10^{-5} \cos(2\psi) + \psi$$

(33)

4. To calculate the equation of time, β (hours):

$$\beta = 0.12357 * \sin(\psi) - 0.004289 * \cos(\psi) + 0.153809 * \sin(2\psi)$$
$$+0.060783 * \cos(2\psi)$$

(34)

5. To calculate the solar hour angle, h (radians):

$$h = \frac{\pi}{12}(t - \beta - 12)$$

(35)

6. To calculate the cosine of the zenith angle of the sun, cos(Z):

$$\cos(Z) = \sin(\phi)\sin(D) + \cos(\phi)\cos(D)\cos(h)$$

(36)

7. To calculate the instantaneous solar energy flux through an area element parallel to the surface at the top of the atmosphere, $q_{SW,atm}$ (W/m^2):

$$q_{SW,atm} = S * \frac{[1 + e * \cos(\theta)]^2}{1 - e^2} * \cos(Z)$$

(37)

Where the inputs are:

φ is the latitude (radians)

d is the day of the year ($1 \leq d \leq 365$)

t is the time of day in hours ($0 \leq h \leq 24$)

S is the solar constant = 1377 W/m^2

e is the ellipticity of the earth's orbit = 0.0167238